GEOCHEMISTRY

Melting of subducted slab dictates trace element recycling in global arcs

Huijuan Li[1], Joerg Hermann[2], Lifei Zhang[1]*

Arc magma acquires continental crust-like trace element signatures through selective recycling of incompatible elements from the subducted slab. The long-standing model of element recycling through aqueous fluid from altered oceanic crust (AOC) and sediment melt has been challenged by the resurgence of mélange diapir (a mix of AOC, sediment, and serpentinite) and saline aqueous fluid models. Here, we present experimental data for near-solidus sediment melts and a framework for calculating trace element concentrations in subduction fluids from metamorphosed sediment and oceanic crust. We observe that variation of element ratios in global primitive arc basalts is comparable with that of sediment and/or oceanic crustal melt, rather than (saline) aqueous fluid or mélange melt. In particular, the systematic correlation of element ratios in arc basalt corresponds to element fractionation in slab melt with temperature and therefore follows a power function. Our findings suggest that slab melt is primarily responsible for element recycling to the arc.

INTRODUCTION

Arc basalt has a major element composition similar to mid-oceanic ridge basalt (MORB) and ocean island basalt, but distinctive trace element characteristics, such as enrichment in large ion lithophile elements (LILEs; e.g., Rb, Cs, Ba, Sr, and Pb), light rare earth elements (LREEs; e.g., La and Ce), Th, U, and depletion in high field strength elements (HFSEs; e.g., Nb, Ta, Zr, and Hf). The enrichment of incompatible trace elements has been attributed to the addition of a subduction component to the mantle wedge [e.g., (*1*, *2*)]; however, the nature of this subduction component and its means of addition remain under debate. Understanding the element recycling mechanism is essential for reconstructing the geodynamic processes at work in subduction zones. One popular hypothesis is that the generation of arc basalt can be modeled with three components: depleted mantle, sediment melt, and aqueous fluid from dehydration of altered oceanic crust (AOC) [e.g., (*3*, *4*)]. This model was derived on the basis of the general negative correlation between LILE/LREE (e.g., Ba/La, Ba/Th, and Pb/Ce) and primitive mantle normalized $(La/Sm)_N$ observed within and among global arcs [Ba/Th versus $(La/Sm)_N$ is shown in Fig. 1A], which has been regarded as the signature of arc basalt geochemistry. LILE/LREE and $(La/Sm)_N$ have been used as proxies for the relative contributions of aqueous fluid from AOC and sediment melt, respectively (*3*, *5*).

There has been a resurgence, in recent years, of both the aqueous fluid addition model (*6*–*8*) and the mélange melting model (*9*–*11*). The renewed interest in the aqueous fluid model is based on the notion that the solubilities of LILE and LREE, but not HFSE, in aqueous fluid increase with salinity. The main argument for the mélange melting model is based on the isotopic conundrum of arc magma, that is, depleted Sr and Pb isotopic ratios in LILE-enriched arc basalts (*1*, *4*). This has traditionally been explained by the addition of an aqueous fluid component from AOC (*4*). The mélange melting model suggests that mechanical mixing of sediment, oceanic crust, and serpentinite (i.e., mélange formation) created the observed isotopic signatures, whereas the fractionation of elements (i.e., the enrichment of LILE) is a result of the melting of mélange diapir in the mantle wedge.

The isotopic compositions (e.g., Nd, Sr, Pb, and ^{10}Be) in arc magma provide unequivocal evidence for sediment contribution (*4*). In the past two decades, the role of slab melting (encompassing the melting of both sediment and oceanic crust) has gained appreciation as a result of some major developments (*12*). Geodynamic modeling suggests that top slab temperatures are high enough to cross the wet solidus for sediment and AOC in most arcs due to the coupling between the subducted slab and the mantle wedge (*13*, *14*). Experimental studies have demonstrated that Cl-poor aqueous fluids from slab dehydration are too dilute to account for the concentration of elements recycled from the subducted slab to arc magma, while sediment melts have been shown to have LILE and LREE contents, and LILE/H_2O and H_2O/LREE ratios comparable with those inferred for arc magmas (*15*, *16*). Concurrently, the dominant role of accessory minerals in controlling the trace element partitioning during slab melting has been gaining recognition (*15*, *17*). In particular, H_2O/Ce and K_2O/H_2O ratios have been used as slab thermometers (*15*, *18*). Top slab temperatures, as predicted by H_2O/Ce and K_2O/H_2O ratios in arc basalts, show excellent agreement with the predictions of geodynamic modeling (*19*). As shown in Fig. 1, both Ba/Th and $(La/Sm)_N$ show good correlations with H_2O/Ce. Therefore, the variation of these element ratios may reflect the variation of slab melts developed at different top slab temperatures.

In this contribution, we investigate the variation of LILE (e.g., Ba and Sr), LREE (La, Ce, and Nd), and H_2O contents, and also LILE/LREE, LILE/H_2O, and H_2O/LREE ratios, in subduction fluids based on new and published experimental results. As these elements are added mainly by the subduction component to the mantle wedge, their overall enrichment patterns in arc magma thus provide important insights into slab processes. A special focus is placed on whether we can distinguish (saline) aqueous fluids, hydrous melts, or intermediate supercritical fluids from sediment or oceanic crust and their contribution to the slab signature of arc magmas.

[1]MOE Key Laboratory of Orogenic Belts and Crustal Evolution, School of Earth and Space Sciences, Peking University, No. 5 Yiheyuan Road, Haidian District, Beijing 100871, China. [2]Institute of Geological Sciences, University of Bern, Baltzerstrasse 1+3, Bern 3012, Switzerland.
*Corresponding author. Email: lfzhang@pku.edu.cn

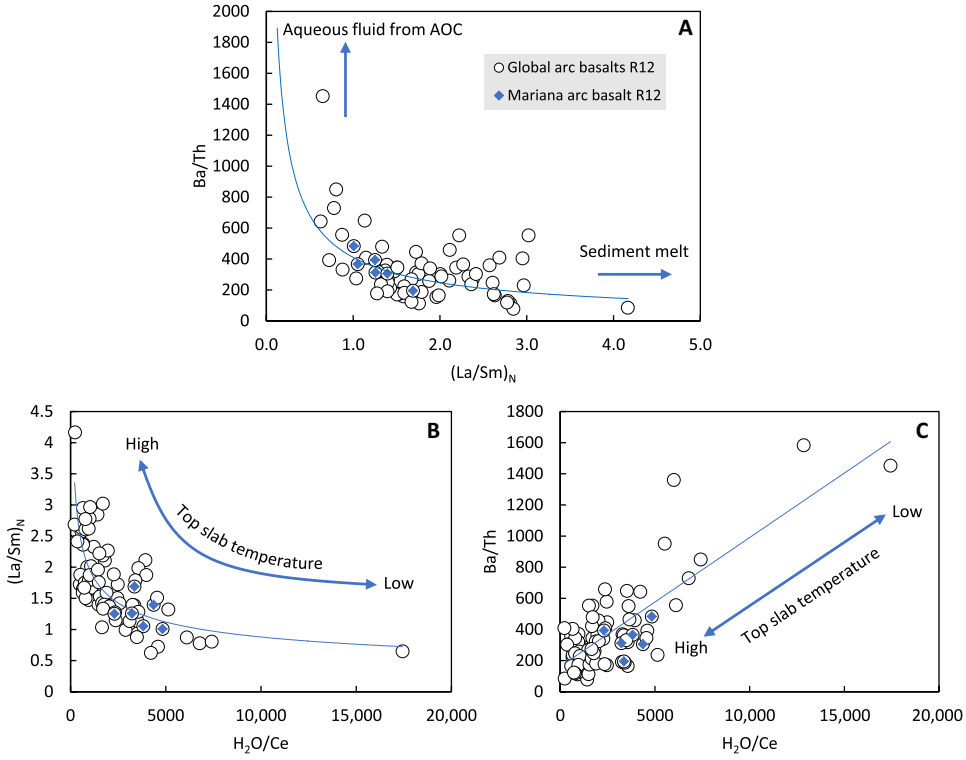

Fig. 1. Negative correlation between Ba/Th and primitive mantle normalized $(La/Sm)_N$ and their correlations with H_2O/Ce in global primitive arc basalts. Data for global arc basalts are from Ruscitto *et al.* (*32*). (**A**) In the three-component mixing model (*3*, *4*), Ba/Th and $(La/Sm)_N$ are used as proxies for the addition of aqueous fluid from AOC and sediment melt, respectively. (**B** and **C**) However, their correlations with H_2O/Ce may reflect their variation in slab melt with top slab temperatures. Trendlines are fitted with power functions in (A) and (B) and a linear function in (C).

RESULTS

Theoretical considerations

Element compatibility during slab melting is often described using bulk partition coefficients $D_i^{\text{residue-melt}}$, which are related to mineral-melt partition coefficients $D_i^{\text{min-melt}}$ as (*20*)

$$D_i^{\text{residue-melt}} = \Sigma D_i^{\text{min-melt}} \times X_{\text{min}} \quad (1)$$

where X_{min} is the mass fraction of mineral phases. Trace element partitioning during slab melting can then be described with a mass balance equation with the form (*21*)

$$D_i^{\text{residue-melt}} \times C_i^{\text{melt}} + C_i^{\text{melt}} \times X_{\text{melt}} = C_i^{\text{bulk}} \quad (2)$$

where C_i^{melt} and C_i^{bulk} represent the concentration of trace element i in melt and the bulk composition, respectively. X_{melt} is the mass fraction of melt. From Eq. 2, melt concentration, when normalized to the bulk composition, can be expressed as

$$(C_i^{\text{melt}})_N = \frac{C_i^{\text{melt}}}{C_i^{\text{bulk}}} = \frac{1}{D_i^{\text{residue-melt}} + X_{\text{melt}}} \quad (3)$$

As can be derived from Eq. 3, $(C_i^{\text{melt}})_N$ for highly incompatible elements (e.g., Cs and Sr) is inversely proportional to melt fraction (*15*, *22*), due to $D_i^{\text{residue-melt}} << X_{\text{melt}}$. When the trace element concerned is the major component in a mineral phase, e.g., K in phengite, Ti in rutile, Zr in zircon, and LREE in allanite/monazite, then $D_i^{\text{residue-melt}} >> X_{\text{melt}}$ and $(C_i^{\text{melt}})_N$ is dominated by the variation of $D_i^{\text{residue-melt}}$ and therefore varies mainly as a function of temperature (*15*, *17*). For elements with moderate incompatibility (e.g., Ba), both the melt and mineral (i.e., mica) fractions are important factors (*15*, *22*).

From Eq. 3, trace element fractionation can be expressed using normalized concentration ratios as

$$\frac{(C_i^{\text{melt}})_N}{(C_j^{\text{melt}})_N} = \frac{D_j^{\text{residue-melt}} + X_{\text{melt}}}{D_i^{\text{residue-melt}} + X_{\text{melt}}} \quad (4)$$

The ratio between highly and moderately incompatible elements, e.g., Sr/Ba, can be approximated as

$$\frac{(C_{\text{Sr}}^{\text{melt}})_N}{(C_{\text{Ba}}^{\text{melt}})_N} \approx \frac{D_{\text{Ba}}^{\text{residue-melt}} + X_{\text{melt}}}{X_{\text{melt}}} = 1 + D_{\text{Ba}}^{\text{residue-melt}} \times \frac{1}{X_{\text{melt}}} \quad (5)$$

The ratio between moderately incompatible and compatible elements, e.g., Ba/La, can be approximated as

$$\frac{(C_{\text{Ba}}^{\text{melt}})_N}{(C_{\text{La}}^{\text{melt}})_N} \approx \frac{D_{\text{La}}^{\text{residue-melt}}}{D_{\text{Ba}}^{\text{residue-melt}} + X_{\text{melt}}} \quad (6)$$

As D_i and D_i/D_j are analogous to the equilibrium constants for element partition and exchange reactions, respectively, thermodynamic considerations suggest linear correlations between $\ln D_i$ and $1/T$ (the inverse of temperature), and between $\ln(D_i/D_j)$ and

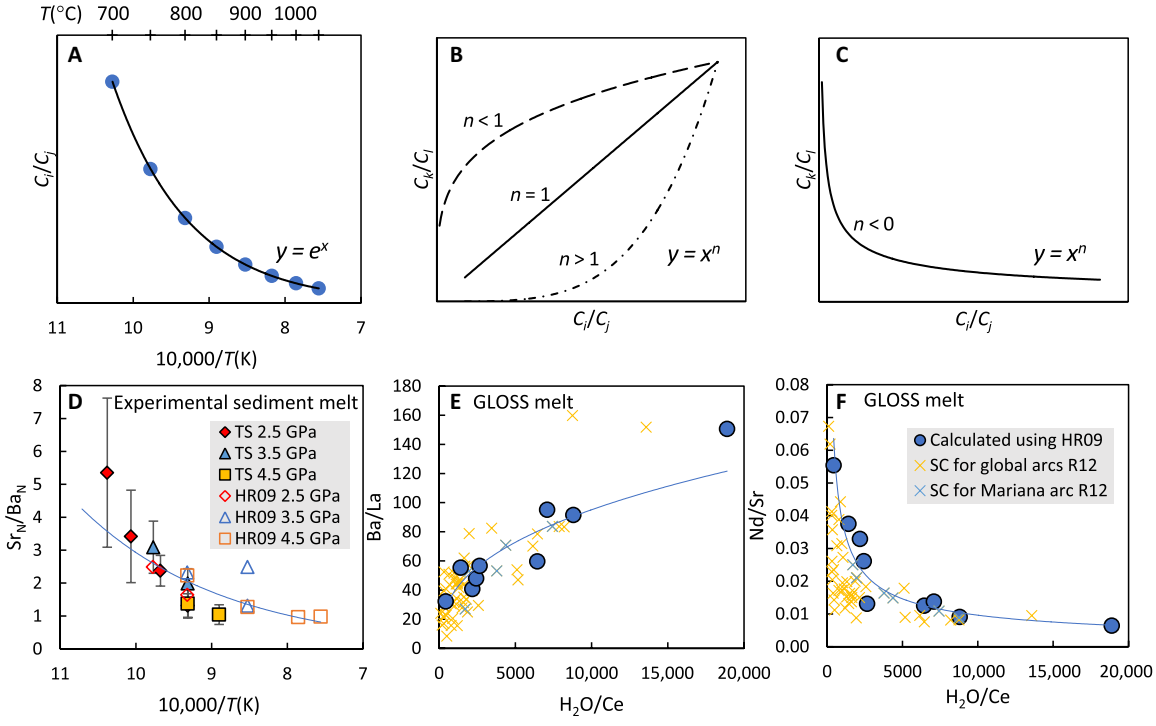

Fig. 2. Trace element fractionation in slab melt due to temperature variation. (**A**) Trace element ratios vary as an exponential function of $1/T$ as depicted schematically. (**B** and **C**) Correlation between element ratios therefore displays as a power function. Given as examples are plots of Sr_N/Ba_N in experimental sediment melt versus $1/T$ (**D**), Ba/La versus H_2O/Ce (**E**), and Nd/Sr versus H_2O/Ce (**F**) for GLOSS melt with element ratios calculated using C_N values from Hermann and Rubatto (*15*). Data plotted in (D) are from this study (TS) and that of Hermann and Rubatto (*15*) (HR09), and form a single trend line fitted with an exponential function. Error bars for the Hermann and Rubatto (*15*) data are smaller than the symbols and therefore not shown. Note the striking comparability between the subduction component (SC) calculated for global arc basalts by Ruscitto *et al.* (*32*) (R12) and GLOSS melt in (E) and (F). The trend lines represent power functions fitted to the GLOSS melt compositions.

$1/T$, i.e., D_i and D_i/D_j are exponential functions of $1/T$. As trace element ratios $(C_i)_N/(C_j)_N$ are proportional to D_j (Eq. 5) or D_j/D_i (Eq. 6), they are also exponential functions of $1/T$, which can be expressed schematically as

$$\frac{(C_i)_N}{(C_j)_N} = e^{a/T} \quad (7)$$

We therefore predict that normalized concentration ratios between two elements $(C_i)_N/(C_j)_N$, with the more incompatible element being the numerator, will show an exponential decrease with decreasing $1/T$ and approach a value of 1 when the compatibility of the two elements converges (i.e., both become incompatible) as temperature increases (Fig. 2A). This is evident in the data from previous sediment melting experiments (see fig. S1) (*15*). Two element ratios, C_i/C_j and C_k/C_l, can therefore be related through a power function (i.e., $y = x^n$)

$$\frac{C_k}{C_l} = e^{b/T} = e^{\frac{b}{a}\times\ln\left(\frac{C_i}{C_j}\right)} = \left(\frac{C_i}{C_j}\right)^{\frac{b}{a}} \quad (8)$$

with a positive slope when the power $n > 0$ (Fig. 2B) and a negative slope when $n < 0$ (Fig. 2C). In this formulation, the variation of element ratios is principally a function of temperature. In the following section, we will use Sr/Ba as an example to demonstrate this in detail.

Sr and Ba fractionation in sediment melt and arc basalt

Ba, Sr, and H_2O in arc magmas are, to a great extent, sourced from the subducted slab. For example, 96 to 98% of Ba and 74 to 94% of Sr in Mariana arc basalts originated from slab contribution (*5*). Therefore, these elements are particularly well suited to constrain the subduction component. Here, we report Ba and Sr contents in sediment melt at pressure and temperature conditions of 2.5 to 4.5 GPa and 690° to 850°C, respectively (table S1). In comparison to previous studies (*15*, *16*), this set of sediment melting experiments (*23*) extends the low-temperature range to just above the wet solidus. Sr content in melt is found to decrease with temperature, and increase with pressure, in accordance with the variation of melt fraction (fig. S2A). This is in clear contrast to a general increase in Ba concentration with temperature (fig. S2B). The effect of varying bulk H_2O content is reflected in the proportional variation of Sr due to the change of melt fraction (fig. S2A), whereas such an effect is negligible for Ba (fig. S2B), which can be attributed to the dominance of D_{Ba} and the counteraction of melt and phengite fractions (Eq. 3). The Sr_N/Ba_N ratio in sediment melt is observed to increase exponentially with increasing $1/T$ (Fig. 2D). It appears that the positive effects of pressure on Sr_N and Ba_N tend to cancel out in the Sr_N/Ba_N ratio. Temperature therefore exerts a first-order control on the variation of Sr_N/Ba_N, while pressure, melt, and phengite fractions play subordinate roles.

The variation of Sr/Ba ratios is apparent in arc basalts from Kamchatka (*24*), which show a clear correlation with either sub-arc

slab depths or top slab temperatures (fig. S3). Such a correlation mimics our experimental observation of Sr/Ba variation with temperature (Fig. 2D). On the other hand, this cannot be explained by the three-component mixing model [e.g., (*3*, *4*)], which suggests that Ba and Sr are both LILE and supposedly sourced from the same AOC aqueous fluid component. The decoupling between Ba and Sr has also been observed in the Aleutian arc, with Ba traced to the subducted sediment melt and Sr attributed to the mixing between sediment melt and an eclogite melt component (*25*–*27*). Variation in the relative contributions of sediment and oceanic crust to the subduction component may certainly cause Ba and Sr fractionation, as in the case of the Aleutian arc, and can only be resolved with additional isotope measurements. Considering the narrow range of Sr isotopic compositions reported (*28*), i.e., the relatively constant ratios between sediment and oceanic crustal contributions to the Sr budget, the variation of Sr/Ba in Kamchatka arc basalts is most likely a result of the variation of top slab temperatures.

Comparability of trace element ratios between slab melt and the subduction component

The derivation of Eqs. 1 to 3 and the concept of bulk composition–normalized element concentration (C_N) can equally be applied to element partitioning involving aqueous fluid or supercritical fluid. First, we established the C_N values from the experimental literature based on reported fluid/melt concentrations and starting compositions. We then calculated trace element concentrations in subduction fluids, namely, melt, aqueous fluid, or supercritical fluid, from both sediment and AOC using these C_N values and by adopting the average global subducting sediment (GLOSS) composition (*29*) and the ODP site 801 "supercomposite" (SUPER) AOC composition (table S2) (*30*). This approach enables comparison between experimental studies that use different trace element concentrations in their starting compositions and the ability to infer the compositions of typical sediment and AOC-derived slab fluids. The usage of C_N values in the calculation of subduction fluid compositions should not be applied in a strict sense to K, Ti, and Zr, when their concentrations in melt are buffered by phengite, rutile, and zircon, respectively. This method works well for LREE due to the fact that allanite is present as an epidote-allanite solid solution (*17*) and monazite can incorporate a varying range of LREE and Th (*31*).

As shown by the plots of Ba/La and Nd/Sr in GLOSS melt against H_2O/Ce (Fig. 2, E and F), the correlation between element ratios can be fitted with a power function, in agreement with the above prediction. When compared to primitive arc basalt compositions for global arcs compiled by Ruscitto *et al.* (*32*), the comparability of element ratios between GLOSS melt and arc basalt is striking (Fig. 2, E and F). Note that these figures use element ratios in the subduction component calculated from primitive arc basalts by Ruscitto *et al.* (*32*) rather than the arc basalt compositions. This is necessary for Nd/Sr, as Nd in arc basalt has a substantial mantle component. For element ratios involving H_2O, Sr, Ba, La, and Ce, which are sourced mainly from the slab, the values are similar between arc basalt and the subduction component.

Given that the correlation between two element ratios follows a power function (Eq. 8), it is instructive to plot such data using a logarithmic scale. As shown by the plots of Ba/La and Nd/Sr against H_2O/Ce in Fig. 3 (A and B), the experimental data from different studies fall on two linear arrays, one for sediment-derived fluids and the other for AOC-derived fluids. It is encouraging to see the coherence of this dataset, as it is derived from different experimental setups, variable analytical techniques, and varying starting compositions. The linear trends reveal similarities and differences between fluids derived from subducted AOC and sediment. Both AOC melt (*17*, *33*) and supercritical fluid (*34*) can have Ba/La and Nd/Sr ratios comparable with those for GLOSS melt (*15*, *35*), while higher H_2O/Ce values result from both the lower Ce content in the SUPER AOC composition and lower $(C_{Ce})_N$ values for AOC melt and supercritical fluid at comparable pressure and temperature conditions (table S2). Aqueous AOC nonsaline fluids (*6*) show not only two to three orders of magnitude higher H_2O/Ce than the subduction component of arc basalts but also Ba/La ratios that are at least an order of magnitude higher. With increasing salinity, H_2O/Ce, Ba/La, and Nd/Sr ratios in AOC aqueous fluids (*6*) approach the values for AOC melt and supercritical fluid, although still higher than those inferred for arc basalts (Fig. 3, A and B). The Ba/La and Nd/Sr ratios in GLOSS aqueous fluid (*36*) are similar to those for GLOSS melt but can be distinguished by their much larger H_2O/Ce ratios due to low Ce contents. The above results highlight the usefulness of H_2O/LREE in combination with LILE/LREE ratios to distinguish different types of subduction fluids. The data points of AOC saline aqueous fluids (*6*) overlap those of the low temperature AOC melts (*33*), and the increase of salinity appears to mimic the effect of increasing temperature (Fig. 3, A and B). Moreover, the AOC saline aqueous fluids (*6*) from 4 GPa and 800°C experiments may be classified as supercritical fluids based on their solute contents, which increase with increasing salinity (*8*). The similarity in Ba/La, Nd/Sr, and H_2O/Ce ratios between AOC saline aqueous fluids (*6*) and AOC supercritical fluids at 5 and 6 GPa, 800°C from Rustioni *et al.* (*8*) supports such an interpretation (fig. S4). The H_2O contents for AOC saline aqueous fluids were calculated as the difference in solute content from 100%, as shown in Fig. 3 (C and D) and table S2. The two AOC nonsaline aqueous fluids with H_2O contents >70 weight % (wt %) lie to the right of the AOC linear array due to their lower Ce contents and higher H_2O/Ce ratios, similar to GLOSS aqueous fluids. Therefore, the AOC array represents AOC melts and supercritical fluids, with element ratios varying over several orders of magnitude. However, only the high-temperature end of the array shows comparable Ba/La and Nd/Sr ratios to those inferred for arc basalts, while the much lower values at the low-temperature end may reflect the control of epidote-group minerals on LREE and Sr partitioning during AOC melting (*33*).

A drawback of using element ratios such as Ba/La is an inherent ambiguity, that is, a high value for Ba/La could arise from either high Ba or low La contents. As the enrichment of LILE is the most characteristic feature of arc basalt, it is essential to compare also non-normalized values of Ba and Sr in subduction fluids with concentrations in arc basalts (Fig. 3, C and D). In these plots, the actual basalt composition is plotted and not the inferred subduction component. Arc basalt can be considered as a mixture of the subduction component and a depleted mantle melt that is situated close to the origin due to the low Sr and Ba contents in the mantle source. The GLOSS melt data (*15*, *35*) plot in the sector of Ba/H_2O ratios compatible with those observed in arc basalts (Fig. 3C). The low Ba contents in AOC melt and fluid reflect the low Ba content in the SUPER AOC composition [865 parts per million (ppm) in GLOSS versus 16.6 ppm in AOC, both anhydrous], despite the fact that Ba behaves as a highly incompatible element in the absence of phengite due to either a K-free starting composition (*6*, *34*) or high bulk H_2O contents (15 to 20 wt %) (*17*, *33*) used in these AOC melting experiments. The

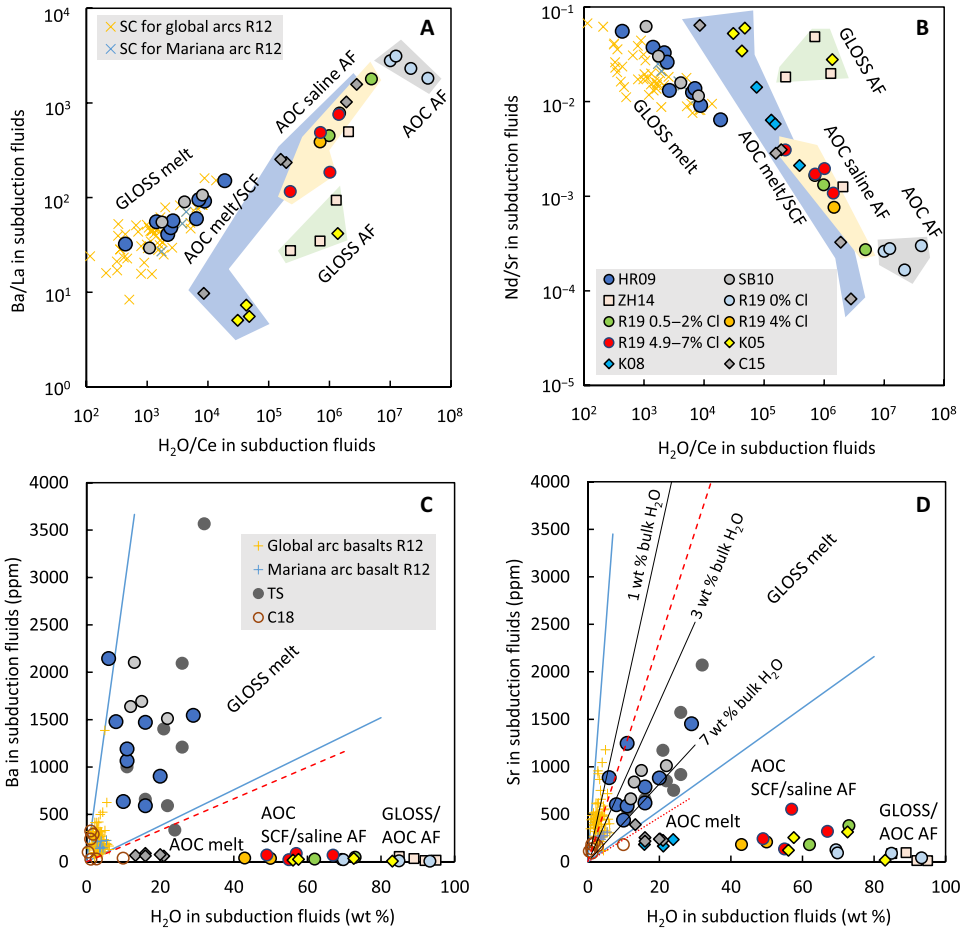

Fig. 3. Trace element comparison between subduction fluids and global primitive arc basalts. Given as examples are plots of Ba/La versus H_2O/Ce (**A**), Nd/Sr versus H_2O/Ce (**B**), Ba versus H_2O (**C**), and Sr versus H_2O (**D**). Data for global arc basalts are from Ruscitto *et al.* (*32*), with Ba/La and Nd/Sr ratios representing the subduction component (SC), and Ba, Sr, and H_2O contents from primitive arc basalt compositions. Experimental C_N values from the literature and this study (TS) were used to estimate the compositions for GLOSS melt (HR09, SB10, and TS) (*15*, *35*), AOC melt (K08 and C15) (*17*, *33*), GLOSS aqueous fluid (AF) (ZH14) (*36*), AOC saline aqueous fluids (R19 followed by salinity value) (*6*), and AOC melt/supercritical fluids (SCF) (K05) (*34*). Experimental data for peridotite + mélange melting (C18) (*10*) are also plotted in (C) and (D) for comparison. Note that the blue lines in (C) and (D) represent the maximum and minimum LILE/H_2O ratios observed in arc basalts. Black trendlines in (D) are calculated Sr contents in GLOSS melt with 7, 3, and 1 wt % bulk H_2O contents according to Hermann and Rubatto (*15*). The red dashed lines in (C) and (D) represent calculated Ba/H_2O and Sr/H_2O ratios in AOC melt with 1 wt % bulk H_2O when $D^{\text{residue-melt}} = 0$, respectively. The red dotted line in (D) is a linear fit of calculated Sr contents in AOC melt with 1 wt % bulk H_2O according to Klimm *et al.* (*17*).

maximum Ba/H_2O ratios for AOC melting with 1 wt % bulk H_2O (red dashed line in Fig. 3C; i.e., when $D^{\text{residue-melt}} = 0$) are still below the minimum Ba/H_2O ratios observed in primitive arc basalts. Moreover, for a MORB composition with 0.4 wt % K_2O and 1.5 to 2 wt % H_2O, phengite may be stable up to 850°C due to the low degree of melting (*37*), which would lead to even lower Ba content in AOC melt. GLOSS aqueous fluid (*36*) also has a low Ba content, despite the higher Ba content in GLOSS. Experimental melts produced by melting of peridotite hybridized by mélanges (*10*) show high and low Ba contents representing 5 to 15% sediment and 15% serpentinite addition, respectively (Fig. 3C).

Although the story for Sr may appear similar to Ba at first glance when comparing Fig. 3, C and D, there are some fundamental differences between their behaviors. The enhancement of Sr concentration in saline aqueous fluids (*6*) is noticeable (Fig. 3D). Nevertheless, when plotted together with H_2O, it is again evident that Sr contents in aqueous fluids from both sediment (*36*) and AOC (*6*) are too low to explain the composition of arc basalts. Unlike Ba, the Sr concentration of mélange melts (*10*) is too low to account for Sr in arc basalts. While Ba is only moderately incompatible due to incorporation in phengite in sediment melting experiments, Sr behaves as a highly incompatible element. The Sr content in melt is therefore inversely proportional to the melt fraction (Eq. 3), which is a function of pressure, temperature, and bulk H_2O content (fig. S2A). As both Sr and H_2O decrease with temperature, and increase with pressure, Sr/H_2O in melt varies mainly as a function of bulk H_2O content. We can therefore fit linear trendlines for GLOSS melting with different bulk H_2O contents to experiments covering a wide range of pressure and temperature conditions (Fig. 3D) (*15*). The trendline for Sr/H_2O in AOC melt (*17*) with 1 wt % bulk H_2O was also calculated (red dotted line in Fig. 3D) and lies just below the minimum Sr/H_2O ratios observed in primitive arc basalts. Therefore, for AOC melt to have comparable Sr/H_2O ratios to those of arc basalts, either a lower degree of melting (<1 wt % bulk H_2O)

or greater Sr incompatibility is required. The maximum Sr/H_2O ratios in AOC melt with 1 wt % bulk H_2O when $D^{residue\text{-}melt} = 0$ are also shown for reference (red dashed line in Fig. 3D).

DISCUSSION

Implications for arc magma genesis

The comparability between LILE/LREE and LILE/H_2O ratios in GLOSS and/or AOC melt/supercritical fluid and the subduction component for global primitive arc basalts (Fig. 3) provides strong evidence that a slab melt/supercritical fluid is required to explain the characteristic LILE enrichment, while the ratios for (saline) aqueous fluids do not match the arc basalt characteristics. We emphasize the importance of using H_2O/LREE and LILE/H_2O ratios to trace the source and character of the subduction fluid phases, as they reflect both the element solubility and the source contribution to the element budget. The notable comparability between Ba/La, Ba/H_2O, and H_2O/Ce ratios in GLOSS melt and arc basalt reflects the fact that sediment dominates the LILE and LREE budget in the subducted slab; therefore, sediment melt is the primary phase responsible for the LILE/LREE fractionation. The contribution of oceanic crust stems from the fact that it is equally important for the Sr and medium rare earth element budget (*38*), which is further indicated by Sr isotopic systematics (see below). The mixing of sediment melt and AOC melt tends to result in the situation where Ba, La, and Ce contents in arc basalt are mainly derived from sediment melt, as their concentrations are higher than AOC melt. Consequently, Ba/La and H_2O/Ce ratios in arc basalt mainly reflect those in sediment melt. Meanwhile, Nd and Sr contents and Nd/Sr ratios may have equally important contributions from both sediment and AOC melts.

The general negative correlation between LILE/LREE and $(La/Sm)_N$ ratios in arc basalt is traditionally explained by mixing between an aqueous fluid component from AOC and sediment melt (*3*, *4*). However, we have demonstrated that AOC aqueous fluid can have high LILE/LREE ratios, but cannot explain the enrichment of LILE in arc basalts. Moreover, arc basalts with high LILE/LREE happen to have low $(La/Sm)_N$ values, and vice versa (Fig. 1A). Unfortunately, in nature, the absolute contributions of the aqueous fluid component from AOC and sediment melt do not necessarily have such a reversed relationship. In the context of the slab melting model, the general negative correlation between LILE/LREE and $(La/Sm)_N$ observed in arc basalt can now be readily explained by the variation of element ratios in slab melt with temperature. Calculated $(La/Sm)_N$ ratios for GLOSS melt show negative correlations with Ba/La ratios (fig. S5). In comparison to LILE/LREE ratios, the situation for $(La/Sm)_N$ is more complex due to the fact that both the subduction component and the mantle contribute to the Sm budget. However, the variation of these element ratios in slab melt likely plays a major role in the general negative correlation between LILE/LREE and $(La/Sm)_N$ observed in global arc basalts. The negative correlation between $(La/Sm)_N$ and H_2O/Ce in arc basalts can be fitted with a power function with the power $n < 0$ (Fig. 1B), in support of such an interpretation.

An enhancement of LILE and LREE concentrations has been observed in saline aqueous fluids; however, H_2O/LILE, H_2O/LREE, and LILE/LREE ratios are still larger than those for arc basalts (Fig. 3), contrary to the previous suggestions (*6*, *8*). Such a discrepancy can be attributed to the usage of experimental $D_i^{residue\text{-}melt/fluid}$ or $D_i^{melt/fluid\text{-}residue}$, rather than C_N values, in previous studies. These bulk D values were often calculated only for major mineral phases of garnet and pyroxene with the addition of rutile (*6*, *8*, *34*). In trace element–doped experiments, the presence of accessory minerals is a norm rather than a rarity, but can often go undetected. A simple mass balance can demonstrate this point clearly. Such a calculation for La and Ce in experiments from Rustioni *et al.* (*6*) has been given as an example (table S3). The omission of accessory minerals, which are major hosts and therefore dominate trace element partitioning, can result in an overestimation of $D_i^{melt/fluid\text{-}residue}$ values by orders of magnitude. Trace element doping at high concentration was often employed to enhance the crystallization of accessory minerals; however, the usage of C_N values ensures that this method of calculation is independent of the original doping level. This is clearly demonstrated by the comparability of Nd/Sr and H_2O/Ce values for AOC melt estimated based on experiments from Klimm *et al.* (*17*) and Carter *et al.* (*33*), with trace element–doped and natural AOC starting compositions, respectively. As shown in Fig. 3B, the data points representing estimations from these two studies form a single trend.

The comparability between different experimental studies arises from the similarity in mineral assemblages controlling trace element partitioning. The starting compositions used in this study and Hermann and Rubatto (*15*) were modeled after the average GLOSS composition. Skora and Blundy (*35*) adopted the radiolarian clay composition (*29*) for their experimental starting material; however, as their experiments produced similar mineral assemblages, C_N values and calculated GLOSS melt compositions are nearly identical to those from Hermann and Rubatto (*15*) (Fig. 3 and table S2). However, C_N values obtained from the experiments of Martindale *et al.* (*39*) are clearly different from other studies (table S2), due to differences in the mineral assemblages. These experiments were performed with natural volcaniclastic sediments from the West Pacific. The oxygen fugacity of their experiments was so high that hematite was present, and biotite and orthopyroxene, rather than phengite, were stable.

One argument put forward in support of the aqueous fluid model is that Cl in aqueous fluid enhances the fractionation between LILE/LREE and HFSE (*6*, *8*). It is worth noting that this effect has also been observed in Cl-bearing sediment melts (*22*) with H_2O/Cl in the range of 25 to 100 (1.6 to 6.4 wt % NaCleq), typical for arc magmas. To corroborate the saline aqueous fluid argument, Keppler (*7*) reported positive correlations between element/H_2O and Cl/H_2O ratios for basaltic melt inclusions from the Kamchatka arc. However, the element/H_2O ratios increase by a factor of 2 to 6 for the whole Cl/H_2O range measured in the inclusions, which is similar to the degree of enhancement of element concentrations in Cl-bearing sediment melts (*22*), and in clear contrast to the orders of magnitude increase observed in saline aqueous fluids (*6*, *8*). On another note, the Cl effect is minor in comparison to the dominant temperature effect on element fractionation in slab melt, for example, H_2O/Ce ratios in GLOSS melt vary over two orders of magnitude from 750° to 1000°C (Fig. 3, A and B).

The Sr isotopic conundrum in arc magma explained by a slab melting model

In light of the comparability between LILE/H_2O, H_2O/LREE, and LILE/LREE ratios in slab melt and arc basalt, we employ a slab melting model involving the addition of sediment and oceanic crustal melts to the mantle wedge to explain the Sr isotopic compositions of

oceanic arc basalt. By plotting Nd/Sr versus $^{87}Sr/^{86}Sr$, Nielsen and Marschall (*9*) suggested that mixing between a depleted MORB mantle (DMM) source with sediment melts or aqueous fluids from the dehydration of AOC cannot produce the range of Nd/Sr ratios observed in arc magmas. However, Nielsen and Marschall (*9*) calculated Nd/Sr ratios in sediment melt based on fixed D_{Nd} and D_{Sr} values. Using the Mariana arc as an example, we calculated Nd/Sr in sediment melt (*15*) and oceanic crustal melts [from both AOC and unaltered oceanic crust ("UOC")] based on experimental C_N values in the temperature range of 750° to 900°C (table S4) (*17*, *33*, *34*) , with results falling in a similar range to that observed in Mariana arc basalt (Fig. 4). The reported sub-arc depth for South Marianas is up to 170 km (*13*), well within the supercritical fluid field for slab melting. Although there are no experimental data for supercritical sediment fluid, AOC supercritical fluids have been shown to have element ratios similar to AOC melt (table S2) (*34*). Therefore, the variation of Nd/Sr in Mariana arc basalt results from the variation of Nd/Sr in the subduction component as a function of temperature. This is corroborated by the negative correlation between Nd/Sr and H_2O/Ce in the Mariana subduction component (Fig. 2F). Considering the possible effect of fractional crystallization (i.e., increasing Nd/Sr with increasing SiO_2; fig. S6), only the basaltic melt compositions are plotted in Fig. 4. Due to a lack of element fractionation at mantle melting temperatures, Nd/Sr ratios produced by mélange melting (*10*) are higher than those for arc basalts (Fig. 4).

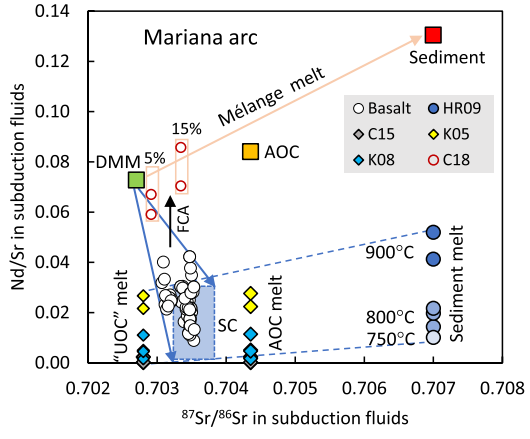

Fig. 4. Illustration of the mixing between DMM and the subduction component (SC) to produce Mariana arc basalts, and the mixing of sediment and oceanic crustal melts to produce SC. Arc basalt compositions are from the Geochemistry of Rocks of the Oceans and Continents (GEOROC) database (http://georoc.mpch-mainz.gwdg.de/georoc/). The Nd and Sr concentration and isotopic data for DMM, Mariana sediment, and AOC are those compiled by Nielsen and Marschall (*9*). The N-MORB composition from Sun and McDonough (*56*) was used to represent unaltered oceanic crust. Nd/Sr ratios in Mariana sediment and oceanic crustal melts were estimated using experimental C_N values from the same sources as in Figs. 2 and 3, in the temperature range of 750° to 900°C. The symbols for sediment melts, calculated on the basis of experiments with the same bulk H_2O content (~7 wt %), are displayed with different shades to highlight the variation of Nd/Sr with temperature. The Nd/Sr and $^{87}Sr/^{86}Sr$ range for SC are estimated on the basis of ~75% subduction contribution to the Sr budget (*5*). It is clear that oceanic crustal melt is dominated by the melting of UOC, which should have a $^{87}Sr/^{86}Sr$ ratio similar to DMM. It has been given a value of 0.7028 for the purpose of illustration. The Nd/Sr ratios for melts produced by DMM + 5/15% sediment melting are estimated on the basis of the experimental C_N values from Codillo *et al.* (*10*) (C18). The black arrow signifies the increase of the Nd/Sr ratio in evolved arc magma due to fractional crystallization and assimilation (FCA).

Calculations by Pearce *et al.* (*5*) indicate that the central island province of the Mariana arc, although depleted in comparison to other parts of the arc, still has, on average, ~75% Sr from subduction contribution. On the basis of such a percentage, the subduction component is estimated to have $^{87}Sr/^{86}Sr$ ratios in the range of ~0.7032 to 0.7038, and Nd/Sr ratios up to ~0.032 (blue field in Fig. 4). The $^{87}Sr/^{86}Sr$ ratios of the subduction component suggest a dominant contribution from the melt of unaltered oceanic crust, which should have a $^{87}Sr/^{86}Sr$ value similar to DMM. Note that Nd/Sr ratios in pristine MORB and AOC are similar (*33*); therefore, the melt of unaltered oceanic crust has Nd/Sr ratios in a similar range to that of AOC melt. As shown in Fig. 3D, the array of Mariana arc basalts falls along the trend line with the lowest Sr/H_2O ratio. This can be well explained by a subduction component consisting of a mixture of slab melts derived from sediment and oceanic crust. As suggested by Hauff *et al.* (*40*), Pb isotopic compositions of Mariana magma can be explained by mixing between a radiogenic endmember represented by sediment and an unradiogenic endmember generated by mixing of ~80% unaltered oceanic crust and ~20% highly altered oceanic crust.

The melting of unaltered oceanic crust has also been proposed for the Aleutian arc (*25*–*27*, *41*), which has been modeled successfully by mixing DMM, sediment melt, and an eclogite melt (*26*, *27*). Such an "eclogite melt" component is equivalent to the melt of unaltered oceanic crust. It is represented by the high-Mg# andesites and dacites in the western Aleutians, which have adakitic trace element patterns and DMM-like isotopic compositions. Although similar andesites and dacites with high Sr and depleted Sr isotopes have been reported mostly in subduction zones involving hot and young slabs (*27*), melting of unaltered oceanic crust may well be a global phenomenon and may represent the underlying cause for the isotopic conundrum of arc magmas.

The appeal of the mélange melting model lies in its simple explanation of the arc magma isotopic conundrum. However, as shown above, this can also be explained successfully with a slab melting model. A major issue with the mélange melting model is the lack of required element fractionation during mélange melting at mantle temperatures (*10*). There seems to be a very large range of mélange compositions (*11*). For example, the mélange trace element compositions not only encompass those for arc magmas but also cover a much more extended range in the plots of Ba/Th versus $(La/Sm)_N$ and Ce/Pb versus Nb/La (*11*). Hence, it is difficult to reconcile the random nature of mélange compositions with the systematic variation of arc magma compositions. Moreover, the concentration of Sr in mélange melts is too low to satisfactorily explain its enrichment in primitive arc basalts (Fig. 3D). The average mélange composition reported by Marschall and Schumacher (*11*), although resembling the trace element patterns of arc magmas, has a negative Sr anomaly (see their figure 1B). The mélange melts thus inherit such a low Sr character due to the lack of element fractionation during mélange melting.

Implications for the conditions of slab melting

As the trace element fractionation observed in slab melt represents a close match to that of arc basalt, a genetic relationship between slab melt and arc basalt is clearly indicated through trace element recycling. Slab melting has direct implications for the thermal

structures of subduction zones. We are not attempting to convert any of these trace element ratios to slab temperatures as there are many other factors that influence the concentrations of these incompatible elements. For example, the variation of experimental bulk H_2O content results in a variation in melt fraction, which has a strong control on the concentration of highly incompatible elements (Fig. 3D). The Sr/H_2O ratios in arc basalt suggest that fluxed melting of sediment and oceanic crust occurs at a low degree with a low bulk H_2O content (Fig. 3D). Lower degrees of melting, in turn, sustain the stability of accessory minerals at lower trace element concentrations in the slab. This implies that trace element partitioning during slab melting in nature is dominated by accessory mineral phases as observed in experimental studies. The importance of accessory minerals in element fractionation during slab melting should not be underestimated, as their absence leads to drastic changes in element behavior, for example, in the studies of Rustioni *et al.* (*6*, *8*) and Kessel *et al.* (*34*), which used K-free oceanic crust starting compositions, Ba behaves as a highly incompatible element due to the absence of mica in the residue. While such experiments produced fluids with high Ba/La ratios (Fig. 3A), the low Ba concentrations fail to explain the characteristic Ba enrichment observed in arc basalts (Fig. 3C). It is worth noting that Rustioni *et al.* (*8*) demonstrated that a lower percentage of 1 to 2 wt % saline fluids (with 5 to 10 wt % Cl) released from eclogite at 4 GPa, 800°C can have higher Ba. The addition of 2.5 to 10 wt % of such a fluid to the locus of mantle wedge melting can produce the Ba enrichment observed in arc magmas (*8*). However, the magmas produced would have high H_2O contents (8 to 32 wt % at 20% partial melting) (*8*), suggesting that H_2O/Ba ratios for such fluids are still too high to match the values observed in arc magmas. This is demonstrated by the trendline for the maximum Ba/H_2O ratios achievable in AOC melt and supercritical fluid with 1 wt % bulk H_2O shown in Fig. 3C.

Fluxed melting of slab crustal sections at sub-arc depth requires an external fluid source, which could originate from the dehydration of serpentinite/chlorite schists atop the slab or slab gabbro/serpentinite. Heavy $\delta^{11}B$ isotopes (*42*) and trace element features (e.g., B, Sb, As, and halogens) in arc magma all point to a serpentinite source (*12*, *43*). The slab melting model highlights the decoupling between slab dehydration and trace element recycling. Fluids released from the dehydrating slab at fore-arc depth may take part in slab melting through the dehydration of down-dragged hydrated mantle wedge or mélange at the slab-mantle interface. As serpentine atop the slab dehydrates completely before reaching 100 km depth (*44*), the dehydration of chlorite may contribute to the fluxed melting of slab crustal sections (*45*). The dehydration of lower crustal gabbro and slab serpentinite may be another fluid source. The migration of fluid produced by the dehydration of serpentinite from the deeper slab mantle through the stratigraphy of the slab can also explain the contribution of unaltered oceanic crust to the subduction component (*46*).

Fluxed melting of the slab crustal sections also requires supersolidus conditions at the locus of melting. This is likely to be the case at the top of the slab at sub-arc depth, as suggested by geodynamic modeling (*13*, *44*); however, it may occur at subsolidus conditions for the lower crustal sections, especially in cold subduction zones. In this case, supercritical fluids may be the dominant medium for element transport if a component from unaltered oceanic crust is identified in the arc magma (*34*).

Although data presented in this study rule out a major role for aqueous fluid in terms of trace element recycling, many studies have suggested that intraslab reactive fluid flow can mobilize trace elements to some extent, as observed in many natural samples representing fore-arc dehydration and fluid migration (*47*–*50*). Such an open system scenario can certainly modify aqueous fluid compositions and generate arc magma signatures (*50*); however, the fluid phase may still have LILE/H_2O and H_2O/LREE ratios representing aqueous fluid characteristics and require H_2O loss through the interaction with the mantle wedge (*8*) to produce the ratios observed in arc magmas. The transport of slab melt to the locus of partial melting in the mantle wedge may result in the formation of hydrous minerals, such as phlogopite and amphibole, which may cause further fractionation of LILE and REE, respectively. In particular, the residual fluid will have lower K_2O/H_2O and higher H_2O/Ce in comparison to arc basalt (*51*). This effect is minimized if slab melt is transferred by focused flow to ensure limited alteration of slab trace element signatures during the transportation process (*51*). While reactive fluid flow modeling in the slab and the mantle wedge is beyond the scope of this paper, it is certainly a fruitful area for future research, such as illustrating the transportation of aqueous fluid and slab melt both intraslab and within the mantle wedge. The framework for calculating trace element compositions in subduction fluids presented here provides geochemical constraints for such modeling.

A simple consideration of element fractionation in slab melt with temperature explains some key trace element characteristics of arc magma effortlessly. We therefore advocate that slab melt from sediment and oceanic crust is the dominant conveyor for mass transfer from the slab to the mantle wedge. We arrive at such a simple model based on general observations of element fractionation in global arc basalts. Its reconcilability with Sr isotopic data has been demonstrated using the Mariana arc as an example. While this model offers an alternative reference scheme for explaining elemental and isotopic compositions of arc magmas, it will benefit from further refinement in future studies. We acknowledge that there are many other factors that need to be taken into consideration in a case-by-case study of individual arcs (*52*) when presented with the full spectrum of elemental and isotopic data, for example, the variation of sediment and oceanic crust compositions (*29*), their absolute and relative contributions (*25*), the heterogeneity of mantle enrichment (*53*), the thermal structure of the mantle wedge (*54*), and the transport mechanisms of slab fluids into the mantle wedge. Heavy rare earth elements and HFSE systematics in arc basalts are likely dominated by mantle wedge fertility and the degree of partial melting. Nevertheless, it has been shown that 20 to 80% Zr and Hf are derived from the slab component (*5*, *52*). It is also important to note that the mantle wedge temperature will impose a strong control on top slab temperatures at sub-arc depth (*13*), possibly leading to correlations of major element data with compatible (dominated by melting in the mantle) (*52*) and incompatible trace element ratios (dominated by melting in the slab). It therefore represents a challenge to disentangle the temperature effect of the mantle wedge from that of the slab. The main purpose of this work was to show not only that K_2O/H_2O and H_2O/Ce ratios in subduction fluids are a function of temperature but also that there is a strong temperature effect on many other trace element ratios (e.g., Sr/Ba, Ba/La, Ba/Th, and Nd/Sr), an essential consideration noticeably absent in numerous previous studies.

MATERIALS AND METHODS

Sr and Ba data acquisition

Sr and Ba data reported in this study were obtained from a set of sediment melting experiments previously reported by Li and Hermann (*23*). For these low-temperature experiments, low degrees of melting inhibited inductively coupled plasma mass spectrometry (ICP-MS) analysis of trace elements in melt. Sr and Ba analyses were performed with an electron microprobe (JEOL JXA 8230) at Peking University. Sr and Ba were analyzed using the "trace element" method, that is, the major element compositions for melts from Li and Hermann (*23*) were given as the matrix. $SrSO_4$ and $BaSO_4$ were used as calibration standards. Melt pools were analyzed with a defocused beam using an acceleration voltage of 15 kV and a beam current of 20 nA. A counting time of 90 s resulted in a detection limit of ~80 ppm for Sr and ~110 ppm for Ba. Due to the low concentrations of TiO_2 (0.12 to 0.42 wt %) in the experimental melts analyzed, the interference between Ba and Ti peaks has negligible effects on Ba analysis, with an estimated 7 to 26 ppm Ba from Ti contribution according to rutile analysis. However, the interference between Sr and Si peaks caused a degree of overestimation for Sr in melt, for example, 10 analyses of Sr in NIST610 returned an average of 703 ± 71 ppm. Correction of such an interference was performed on the basis of the recommended NIST610 Sr content of 515.5 ± 0.5 ppm (*55*). The Ba and Sr results show good agreement with laser ablation ICP-MS analytical data for experiment C3269 (table S1) (*22*).

SUPPLEMENTARY MATERIALS

Supplementary material for this article is available at https://science.org/doi/10.1126/sciadv.abh2166

REFERENCES AND NOTES

1. C. J. Hawkesworth, K. Gallagher, J. M. Hergt, F. McDermott, Mantle and slab contributions in ARC magmas. *Annu. Rev. Earth Planet. Sci.* **21**, 175–204 (1993).
2. E. Stolper, S. Newman, The role of water in the petrogenesis of Mariana trough magmas. *Earth Planet. Sci. Lett.* **121**, 293–325 (1994).
3. T. Elliott, T. Plank, A. Zindler, W. White, B. Bourdon, Element transport from slab to volcanic front at the Mariana arc. *J. Geophys. Res. Solid Earth.* **102**, 14991–15019 (1997).
4. T. Elliott, in *Inside the Subduction Factory*, J. M. Eiler, Ed. (Geophysical Monograph Series Vol.138, AGU, 2003), pp. 23–45.
5. J. A. Pearce, R. J. Stern, S. H. Bloomer, P. Fryer, Geochemical mapping of the Mariana arc-basin system: Implications for the nature and distribution of subduction components. *Geochem. Geophys. Geosyst.* **6**, Q07006 (2005).
6. G. Rustioni, A. Audétat, H. Keppler, Experimental evidence for fluid-induced melting in subduction zones. *Geochem. Perspect. Lett.* **11**, 49–54 (2019).
7. H. Keppler, Fluids and trace element transport in subduction zones. *Am. Mineral.* **102**, 5–20 (2017).
8. G. Rustioni, A. Audetat, H. Keppler, The composition of subduction zone fluids and the origin of the trace element enrichment in arc magmas. *Contrib. Mineral. Petrol.* **176**, 51 (2021).
9. S. G. Nielsen, H. R. Marschall, Geochemical evidence for mélange melting in global arcs. *Sci. Adv.* **3**, e1602402 (2017).
10. E. A. Codillo, V. Le Roux, H. R. Marschall, Arc-like magmas generated by mélange-peridotite interaction in the mantle wedge. *Nat. Commun.* **9**, 2864 (2018).
11. H. R. Marschall, J. C. Schumacher, Arc magmas sourced from mélange diapirs in subduction zones. *Nat. Geosci.* **5**, 862–867 (2012).
12. C. Spandler, C. Pirard, Element recycling from subducting slabs to arc crust: A review. *Lithos* **170-171**, 208–223 (2013).
13. E. M. Syracuse, P. E. van Keken, G. A. Abers, The global range of subduction zone thermal models. *Phys. Earth Planet. Inter.* **183**, 73–90 (2010).
14. P. E. van Keken, B. Kiefer, S. M. Peacock, High-resolution models of subduction zones: Implications for mineral dehydration reactions and the transport of water into the deep mantle. *Geochem. Geophys. Geosyst.* **3**, 1056 (2002).
15. J. Hermann, D. Rubatto, Accessory phase control on the trace element signature of sediment melts in subduction zones. *Chem. Geol.* **265**, 512–526 (2009).
16. J. Hermann, C. J. Spandler, Sediment melts at sub-arc depths: An experimental study. *J. Petrol.* **49**, 717–740 (2008).
17. K. Klimm, J. D. Blundy, T. H. Green, Trace element partitioning and accessory phase saturation during H_2O-saturated melting of basalt with implications for subduction zone chemical fluxes. *J. Petrol.* **49**, 523–553 (2008).
18. T. Plank, L. B. Cooper, C. E. Manning, Emerging geothermometers for estimating slab surface temperatures. *Nat. Geosci.* **2**, 611–615 (2009).
19. L. B. Cooper, D. M. Ruscitto, T. Plank, P. J. Wallace, E. M. Syracuse, C. E. Manning, Global variations in H_2O/Ce: 1. Slab surface temperatures beneath volcanic arcs. *Geochem. Geophys. Geosyst.* **13**, Q03024 (2012).
20. D. M. Shaw, Trace element fractionation during anatexis. *Geochim. Cosmochim. Acta* **34**, 237–243 (1970).
21. P. W. Gast, Trace element fractionation and the origin of tholeiitic and alkaline magma types. *Geochim. Cosmochim. Acta* **32**, 1057–1086 (1968).
22. H. Li, J. Hermann, The effect of fluorine and chlorine on trace element partitioning between apatite and sediment melt at subduction zone conditions. *Chem. Geol.* **473**, 55–73 (2017).
23. H. Li, J. Hermann, Apatite as an indicator of fluid salinity: An experimental study of chlorine and fluorine partitioning in subducted sediments. *Geochim. Cosmochim. Acta* **166**, 267–297 (2015).
24. M. Portnyagin, K. Hoernle, P. Plechov, N. Mironov, S. Khubunaya, Constraints on mantle melting and composition and nature of slab components in volcanic arcs from volatiles (H2O, S, Cl, F) and trace elements in melt inclusions from the Kamchatka Arc. *Earth Planet. Sci. Lett.* **255**, 53–69 (2007).
25. P. B. Kelemen, G. M. Yogodzinski, D. W. Scholl, in *Inside the Subduction Factory*, J. M. Eiler, Ed. (2003), pp. 223–276.
26. G. M. Yogodzinski, S. T. Brown, P. B. Kelemen, J. D. Vervoort, M. Portnyagin, K. W. W. Sims, K. Hoernle, B. R. Jicha, R. Werner, The role of subducted basalt in the source of island arc magmas: Evidence from seafloor lavas of the western Aleutians. *J. Petrol.* **56**, 441–492 (2015).
27. G. M. Yogodzinski, P. B. Kelemen, K. Hoernle, S. T. Brown, I. Bindeman, J. D. Vervoort, K. W. W. Sims, M. Portnyagin, R. Werner, Sr and O isotopes in western Aleutian seafloor lavas: Implications for the source of fluids and trace element character of arc volcanic rocks. *Earth Planet. Sci. Lett.* **475**, 169–180 (2017).
28. A. Simon, G. M. Yogodzinski, K. Robertson, E. Smith, O. Selyangin, A. Kiryukhin, S. R. Mulcahy, J. D. Walker, Evolution and genesis of volcanic rocks from Mutnovsky Volcano, Kamchatka. *J. Volcanol. Geotherm. Res.* **286**, 116–137 (2014).
29. T. Plank, C. H. Langmuir, The chemical composition of subducting sediment and its consequences for the crust and mantle. *Chem. Geol.* **145**, 325–394 (1998).
30. K. A. Kelley, T. Plank, J. Ludden, H. Staudigel, Composition of altered oceanic crust at ODP Sites 801 and 1149. *Geochem. Geophys. Geosyst.* **4**, 8910 (2003).
31. S. Skora, J. Blundy, Monazite solubility in hydrous silicic melts at high pressure conditions relevant to subduction zone metamorphism. *Earth Planet. Sci. Lett.* **321-322**, 104–114 (2012).
32. D. M. Ruscitto, P. J. Wallace, L. B. Cooper, T. Plank, Global variations in H_2O/Ce: 2. Relationships to arc magma geochemistry and volatile fluxes. *Geochem. Geophys. Geosyst.* **13**, Q03025 (2012).
33. L. B. Carter, S. Skora, J. D. Blundy, J. C. M. De Hoog, T. Elliott, An experimental study of trace element fluxes from subducted oceanic crust. *J. Petrol.* **56**, 1585–1606 (2015).
34. R. Kessel, M. W. Schmidt, P. Ulmer, T. Pettke, Trace element signature of subduction-zone fluids, melts and supercritical liquids at 120–180 km depth. *Nature* **437**, 724–727 (2005).
35. S. Skora, J. Blundy, High-pressure hydrous phase relations of radiolarian clay and implications for the involvement of subducted sediment in arc magmatism. *J. Petrol.* **51**, 2211–2243 (2010).
36. Y. F. Zheng, J. Hermann, Geochemistry of continental subduction-zone fluids 9. Multidisciplinary geofluid processes in subduction zones and mantle dynamics. *Earth Planets Space* **66**, 93 (2014).
37. M. W. Schmidt, D. Vielzeuf, E. Auzanneau, Melting and dissolution of subducting crust at high pressures: The key role of white mica. *Earth Planet. Sci. Lett.* **228**, 65–84 (2004).
38. E. Tenthorey, J. Hermann, Composition of fluids during serpentinite breakdown in subduction zones: Evidence for limited boron mobility. *Geology* **32**, 865–868 (2004).
39. M. Martindale, S. Skora, J. Pickles, T. Elliott, J. Blundy, R. Avanzinelli, High pressure phase relations of subducted volcaniclastic sediments from the west pacific and their implications for the geochemistry of Mariana arc magmas. *Chem. Geol.* **342**, 94–109 (2013).
40. F. Hauff, K. Hoernle, A. Schmidt, Sr-Nd-Pb composition of Mesozoic Pacific oceanic crust (Site 1149 and 801, ODP Leg 185): Implications for alteration of ocean crust and the input into the Izu-Bonin-Mariana subduction system. *Geochem. Geophys. Geosyst.* **4**, 8913 (2003).
41. G. M. Yogodzinski, O. N. Volynets, A. V. Koloskov, N. I. Seliverstov, V. V. Matvenkov, Magnesian andesites and the subduction component in a strongly calc-alkaline series at Piip Volcano, far western Aleutians. *J. Petrol.* **35**, 163–204 (1994).

42. M. Scambelluri, S. Tonarini, Boron isotope evidence for shallow fluid transfer across subduction zones by serpentinized mantle. *Geology* **40**, 907–910 (2012).
43. P. D. Noll, H. E. Newsom, W. P. Leeman, J. G. Ryan, The role of hydrothermal fluids in the production of subduction zone magmas: Evidence from siderophile and chalcophile trace elements and boron. *Geochim. Cosmochim. Acta* **60**, 587–611 (1996).
44. P. E. van Keken, B. R. Hacker, E. M. Syracuse, G. A. Abers, Subduction factory: 4. Depth-dependent flux of H_2O from subducting slabs worldwide. *J. Geophys. Res.* **116**, B01401 (2011).
45. J. Hermann, S. Lakey, Water transfer to the deep mantle through hydrous, Al-rich silicates in subduction zones. *Geology* **49**, 911–915 (2021).
46. S. Chen, R. C. Hin, T. John, R. Brooker, B. Bryan, Y. Niu, T. Elliott, Molybdenum systematics of subducted crust record reactive fluid flow from underlying slab serpentine dehydration. *Nat. Commun.* **10**, 4773 (2019).
47. P. Herms, T. John, R. J. Bakker, V. Schenk, Evidence for channelized external fluid flow and element transfer in subducting slabs (Raspas Complex, Ecuador). *Chem. Geol.* **310-311**, 79–96 (2012).
48. S. Taetz, T. John, M. Bröcker, C. Spandler, Fluid–rock interaction and evolution of a high-pressure/low-temperature vein system in eclogite from New Caledonia: Insights into intraslab fluid flow processes. *Contrib. Mineral. Petrol.* **171**, 90 (2016).
49. A. Beinlich, R. Klemd, T. John, J. Gao, Trace-element mobilization during Ca-metasomatism along a major fluid conduit: Eclogitization of blueschist as a consequence of fluid-rock interaction. *Geochim. Cosmochim. Acta* **74**, 1892–1922 (2010).
50. T. Zack, T. John, An evaluation of reactive fluid flow and trace element mobility in subducting slabs. *Chem. Geol.* **239**, 199–216 (2007).
51. C. Pirard, J. Hermann, Focused fluid transfer through the mantle above subduction zones. *Geology* **43**, 915–918 (2015).
52. M. W. Schmidt, O. Jagoutz, The global systematics of primitive arc melts. *Geochem. Geophys. Geosyst.* **18**, 2817–2854 (2017).
53. E. Todd, J. B. Gill, R. J. Wysoczanski, J. Hergt, I. C. Wright, M. I. Leybourne, N. Mortimer, Hf isotopic evidence for small-scale heterogeneity in the mode of mantle wedge enrichment: Southern Havre Trough and South Fiji Basin back arcs. *Geochem. Geophys. Geosyst.* **12**, Q09011 (2011).
54. S. J. Turner, C. H. Langmuir, R. F. Katz, M. A. Dungan, S. Escrig, Parental arc magma compositions dominantly controlled by mantle-wedge thermal structure. *Nat. Geosci.* **9**, 772–776 (2016).
55. N. J. G. Pearce, W. T. Perkins, J. A. Westgate, M. P. Gorton, S. E. Jackson, C. R. Neal, S. P. Chenery, A compilation of new and published major and trace element data for NIST SRM 610 and NIST SRM 612 glass reference materials. *Geostand. Geoanal. Res.* **21**, 115–144 (1997).
56. S.-s. Sun, W. F. McDonough, Chemical and isotopic systematics of oceanic basalts: Implications for mantle composition and processes. *Geol. Soc. London Spec. Publ.* **42**, 313–345 (1989).

Acknowledgments: We thank S. Nielsen for sharing the Mariana arc data used by Nielsen and Marschall (*9*), M. Wille and M. Tang for comments on an earlier version of the manuscript, M. Tian for discussion regarding reactive fluid flow modeling, and J. Jones for input toward the final manuscript. Constructive reviews by G. Yogodzinski and T. John and suggestions from editor G. Gaetani were appreciated. **Funding:** This study was supported by National Key Research and Development Program of China grant 2019YFA0708501 (to L.Z.) and Swiss National Science Foundation grant 200021_169062 (to J.H.). **Author contributions:** Conceptualization: H.L. and J.H. Methodology: H.L. and J.H. Investigation: H.L. Visualization: H.L. Supervision: J.H. and L.Z. Writing—original draft: H.L. Writing—review and editing: J.H. and L.Z. **Competing interests:** The authors declare that they have no competing interests. **Data and materials availability:** All data needed to evaluate the conclusions in the paper are present in the paper and/or the Supplementary Materials.

Submitted 27 February 2021
Accepted 19 November 2021
Published 12 January 2022
10.1126/sciadv.abh2166

ScienceAdvances

Melting of subducted slab dictates trace element recycling in global arcs

Huijuan LiJoerg HermannLifei Zhang

Sci. Adv., 8 (2), eabh2166. • DOI: 10.1126/sciadv.abh2166

Science Advances (ISSN) is published by the American Association for the Advancement of Science. 1200 New York Avenue NW, Washington, DC 20005. The title *Science Advances* is a registered trademark of AAAS.